Biomed Microdevices (2009) 11:861–867
DOI 10.1007/s10544-009-9303-y

A robust, electrochemically driven microwell drug delivery system for controlled vasopressin release

Aram J. Chung · Yun Suk Huh · David Erickson

Published online: 8 April 2009

Abstract Micro-electro-mechanical-system (MEMS) based implantable drug delivery devices represent a promising approach to achieving more precise dosing, faster release and better localization of therapeutic compounds than is possible with existing technology. Despite recent advancements, there remain challenges in being able to build systems that enable active control over the dose rate and release time, in a robust, low power but simple to fabricate package. Here we demonstrate an implantable microreservoir device that enables delivery of dose volumes as high as 15 μl using an electrochemically based transport mechanism. This approach allows for a significant reduction in the amount of time required for drug delivery as well as reducing the dependence on the external physiological conditions. We present the overall design, operating principle and construction of the device, and experimental results showing the volume transport rate as a function of the strength of the applied electric field. The concentration profile *vs.* time, the power consumption, and ejection efficiency are also investigated. To demonstrate the medical utility of the device we also characterize the *in-vitro* release of vasopressin.

Keywords Drug delivery · Microfluidics · Electrochemical reaction · Vasopressin · Microwell

Electronic supplementary material The online version of this article (doi:10.1007/s10544-009-9303-y) contains supplementary material, which is available to authorized users.

A. J. Chung · Y. S. Huh · D. Erickson (✉)
Sibley School of Mechanical and Aerospace Engineering,
Cornell University,
Ithaca, NY 14853, USA
e-mail: de54@cornell.edu

1 Introduction

Vasopressin (Cys-Tyr-Phe-Gln-Asn-Cys-Pro-Arg-Gly-NH_2) is a peptide hormone synthesized in the hypothalamus and stored/secreted in the posterior pituitary. Administration of vasopressin induces changes in the arterial blood pressure by increasing the resistance of the peripheral vessels (Lienhart et al. 2008). In healthy individuals the effect is often negligible; however it can become a crucial compensatory mechanism for restoring blood pressure during hemorrhagic shock (Lienhart et al. 2008; Peitzman et al. 1995). At present, the primary treatment for hemorrhagic shock is fluid replacement; however this is sub-optimal (Roberts et al. 2001), since it may worsen the patient's condition by dilution of the coagulant (Bickell et al. 1991; Milles et al. 1966; Shaftan et al. 1964; Stern et al. 1993). As an alternative therapy, Morales et al. (1999) reported a set of canine experiments where vasopressin levels showed a marked increase at the onset of blood loss followed by a fall to well below the normal physiological level. Voelckel et al. (2000) and Lindner et al. (1995) demonstrated that the administration of vasopressin improved the survival rate in porcine cases and more recently Krismer et al. (2005) reported for human as well. Excessive doses of vasopressin however have been known to induce injuries to the gastrointestinal tract, skin, myocardium and liver (Malay et al. 2004; Yoo et al. 2007). Administration of vasopressin therefore represents a potential life-saving treatment for hemorrhagic shock upon its replenishment but it should be delivered rapidly and with precise timing to avoid side effects.

The need to enable more precise dosing control, rapid delivery and better microscopic localization over the release of a therapeutic compound (LaVan et al. 2003; Maloney et al. 2005) has led to the development of a number of

different microsystem based technologies including microneedles, micropumps, microparticles, and micro-reservoirs. When compared with some of these other procedures, microneedles and micropumps tend to have more complex fabrication steps and operational procedures resulting in less robust systems. Microparticle based technologies typically comprise of a small particle with an internal cavity that is loaded with the drug (Ahmed et al. 2001; Ahmed et al. 2002) and covered by a cap. This cap dissolves over time releasing the contents at a rate determined by the system chemistry. Polymer micro-reservoir systems consist of a physical mixture of the drug and a biodegradable polymer (Grayson et al. 2004a; Grayson et al. 2005) so that the ratio between two components dictates the release kinetics and diffusion rate. In these passive systems chemical release is initiated immediately after implantation and continues until the on-board dose is depleted. In contrast active micro-reservoir systems enable control over the mechanism that initiates drug release (Grayson et al. 2004b; Prescott et al. 2006). This is typically done either through electrochemical (Santini et al. 1999) or eletrothermal (Maloney et al. 2005) dissolution of a capping membrane. Chung et al. (2008) recently demonstrated the ability to add dose rate control to such systems through the use of electrokinetic transport. At present however such systems are limited to relatively small dose volumes (on the order of 100 nl) and by a dependence on favorable external physiological conditions (*e.g.* no biofouling) in order to allow the contents to be delivered.

In this work, we present an implantable silicon micro-reservoir device that enables delivery of dose volumes as high as 15 μl using a more robust electrochemical transport mechanism. Briefly, the delivery mechanism is based on the use of an electrolytic reaction driven between the capping membrane and another electrode located inside the reservoir. When the reaction is initiated, gold dissolution causes a gradual loss of the mechanical integrity of the capping membrane which eventually ruptures and opens. Gas released during the electrolytic reaction builds up the pressure in the reservoir which then forces the contents out of the well, independent of the external environmental conditions. We demonstrate herein that this approach also allows for a significant reduction in the amount of time required to eject well contents over earlier devices. In this paper, we present the overall design, operation principle and construction of the device, and experimental results showing the volume transport rate as a function of the strength of the applied electric field. The concentration profile *vs.* time, the power consumption, and ejection efficiency are also investigated. To demonstrate the medical utility of the device we also characterize the *in-vitro* release of vasopressin.

2 Materials and methods

2.1 Device fabrication and assembly

The microfluidic device structure used here is a modification of that presented by Chung et al. (2008) and used to control the flight metabolic output of insects in Chung and Erickson (2009). A 3D schematic of the device is shown in Fig. 1. All fabrication procedures described below are based on standard MEMS processes (Judy 2001). Briefly, starting with (100) silicon wafer, silicon nitride is deposited on both sides of the wafer and the backside was etched to define the bottom of a microwell reservoir. Subsequently, gold electrodes were evaporated using an image reversal contact lithography process, and then a polyimide dielectric layer was spun on and etched so as to expose the electrodes and isolate the leads. The pyramidal microwells were then defined by immersing the wafer in potassium hydroxide (Fig. 1(C)) and the remaining silicon nitride underneath the

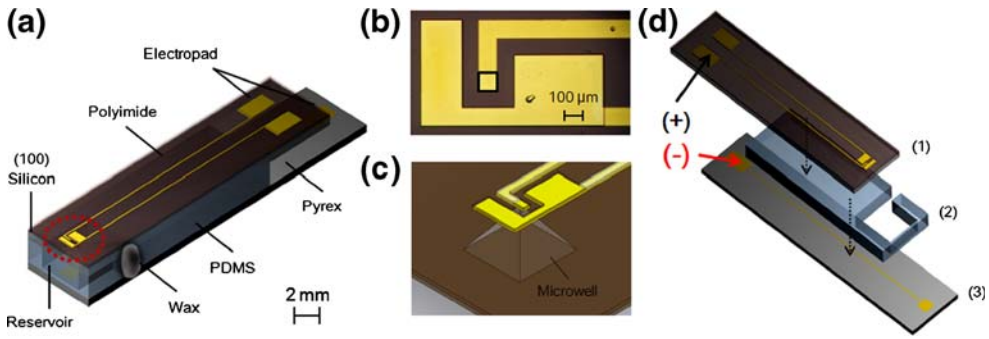

Fig. 1 (**a**) Schematic representative of the electrochemically enhanced microfluidic drug delivery device developed here. The device measures 4.4×2.3×22 mm ($w \times h \times l$). (**b**) Magnified view of microchip from above looking at the region near the membrane. Black square box represents the capping gold membrane. (**c**) Magnified view near fabricated microwell. (**d**) Microchip assembly: (1) an upper silicon based structure (2) PDMS macro-reservoir (3) gold electrode on top of Pyrex substrate. All layers are bonded together by plasma oxidation

gold membrane was removed by reactive ion etching. To create the high volume macro-reservoir a scalpel patterned PDMS spacer was placed between the upper silicon chip and the lower Pyrex support. The approach is based on that developed by Li et al. (2005) who used a similar approach to create a Pyrex macro-reservoir. The use of PDMS here however allows us to simplify device fabrication (by eliminating hydrofluoric acid based glass etching or machining steps) and facilitate assembly (by eliminating wafer bonding steps). Finally the electrode pads and leads on the bottom Pyrex layer were fabricated through gold deposition and standard lift-off processing. Note that the biocompatibility of all the materials used here have been thoroughly investigated by others in a series of recent studies (Voskerician et al. 2003; Richardson et al. 1993; Dokmeci et al. 1997; Belanger and Marois 2001).

To assemble the device the upper (silicon), middle (PDMS), and bottom (Pyrex) substrates were air plasma treated, placed in conformal contact and then stored in an 80°C oven overnight. After this bounding process was complete, the macro-reservoir was filled with the desired chemicals using microsyringe (1705TLL, Hamilton, NV, USA) through a prefabricated side slit. The slit was then sealed with biocompatible wax (Butler GUM, Sunstar, IL, USA) as illustrated in Fig.1(A). After this, the electrode leads were connected to thin copper wires using silver conductive epoxy (M.G. Chemicals, Surrey, BC, Canada). As shown in our recent work (Chung and Erickson 2009), for long term stability the PDMS surface must be coated with Parylene (or a similar hydrophobic material, Shin et al. 2003) in order to minimize fluid loss into the water permeable PDMS substrate. In addition, to minimize the physiological response upon implantation (Ratner et al. 2004; Voskerician et al. 2003), a surface modification, for example, PEG (Polyethylene glycol) should be applied as we have done in the past (Chung and Erickson 2009). Comprehensive, long term tests of the device were not conducted here however it was found that in all cases the devices remained operable for at least a week after surface modifications.

2.2 Vasopressin transport: visualization and quantification

To visualize and quantify the chemical release, fluorescein isothiocyanate (FITC) tagged vasopressin was used. A fluorescein labeling kit and the vasopressin (Arg8-vasopressin) were purchased from Dojindo (Rockville, MD, USA) and Sigma-Aldrich (St. Louis, MO, USA), respectively. FITC was dissolved in 10 μl dimethyl sulfoxide (DMSO) and 8 μl of this solution was well mixed with 100 μl of reaction buffer. After this, the sample was incubated at 37°C for 10 min and 100 μl of 100 mM phosphate buffered saline (PBS) was added to a filtration tube and centrifuged. Since the molecular weight of the vasopressin is relatively small (~1kD), we used Microsep™ centrifugal devices (Pall Corporation, East Hills, NY, USA). The tube was centrifuged at 8000 rpm for 12 h at 4° C. Lastly, 200 μl PBS was added to the FITC-vasopressin conjugation and the final mixture was transferred to a 0.5 ml tube and stored at 4°C. The FITC-vasopressin conjugation was diluted to the appropriate concentrations described below in 100 mM PBS containing 0.145 M of chloride ions (pH 7.4) which was reasonably close to the chloride concentration in human blood (Fitzsimons and Sendroy 1961). The transport of the fluorescein was recorded using Unibrain Fire-i™ software and a Sony XCD-X710 (Tokyo, Japan) camera.

The amount of vassopressin ejected from the devices was quantified via a protein assay using the BCA™Protein Assay Kit (Pierce, Rockford, IL, USA). The assays were performed using a 96-well plate (Corning, Corning, NY, USA), and absorbance was measured at 562 nm by SPECTRAmax 384 (Molecular Devices, Sunnyvale, CA, USA). The vasopressin concentration was calculated from the bovine serum albumin (BSA) standard curve.

2.3 Device design and operation principle

A diagram of the device operation is shown in Fig. 2. The PDMS reservoir and microwell contain approximately 15 μl of 0.05 g/l vasopressin for release. When drug release is desired, an electrical potential is applied between upper and lower electrodes, as shown in Fig. 1(D), resulting in two electrochemical reactions which affect the ejection process. First, the presence of a small amount of chloride ions in the buffer solution creates a water-soluble chlorogold complex from the gold membrane (Frankenthal and Siconolfi 1982) (this was similarly demonstrated by Santini et al. (1999)). This results in a gradual loss of the mechanical integrity of the membrane (due to dissolution of the gold) which eventually ruptures, exposing the contents to the external environment. Simultaneously, the two electrodes also serve as an anode and cathode for electrolysis of water. Gas released during this reaction results in an increased pressure in the reservoir which pushes the liquid contents out through the dissolved membrane. More details on the electrochemical reaction are available in the supplemental material. In all cases, a Keithley 236 Source-Measure Unit (Cleveland, OH) was used to apply these potentials and to measure the current load.

3 Results and discussion

3.1 Electrochemically driven ejection

The electrochemical transport mechanism was demonstrated for two different interface conditions: the first being for the drugs ejected directly into the air and the other is the

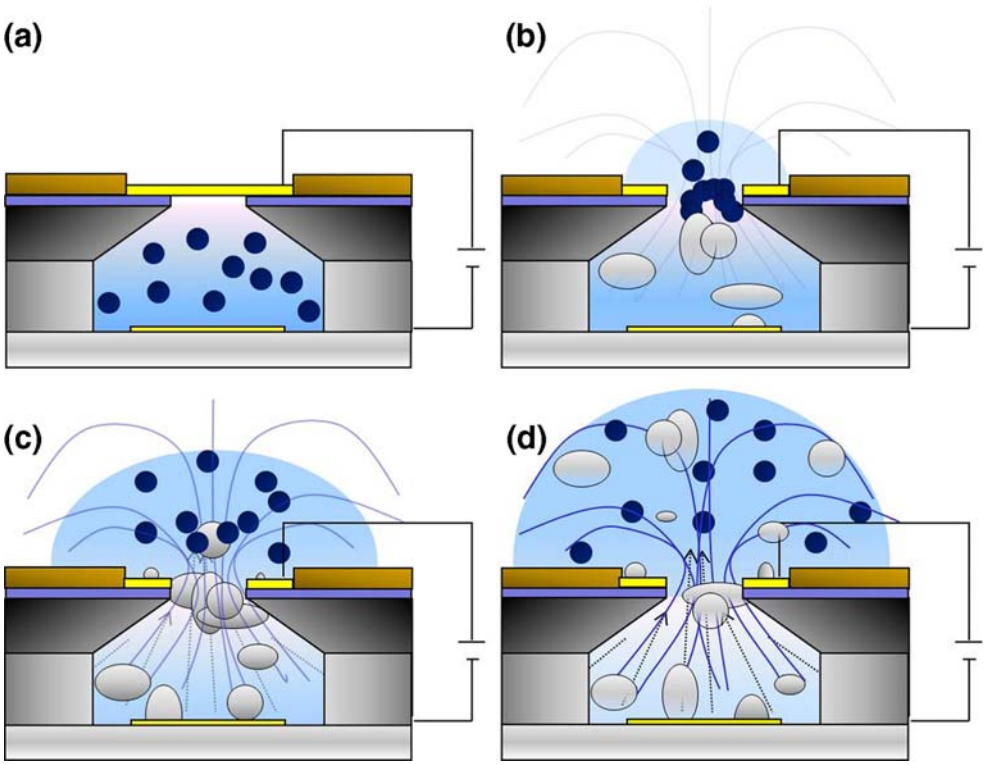

Fig. 2 Scheme describing the operational stages of the electrochemically driven microfluidic drug delivery device (not to scale). (**a**) The electric potential is applied between top and bottom electrodes and current flows through the reservoir independent of the surrounding environment. (**b**) Two main electrochemical reactions occur: dissolution of the gold membrane and electrolysis or water resulting in gas release. (**c**) The generated microbubbles propel well contents out. (**d**) The reaction continues until fluid transport stops

chemicals ejects into a fluid solution surrounding the gold membrane. As mentioned in the introduction, one of the most significant limitations to the development of implantable drug delivery devices is the uncertain physiological conditions that will be faced upon implantation. Many of the passive devices discussed above are compatible with specific solution-phase environmental conditions (*e.g.* polymer based biodegradable systems) and thus suffer from significant performance degradation due to, for example, biofouling (Ratner et al. 2004; Voskerician et al. 2003). One of the major advantages of the electrochemical reaction based device developed here, is that allows us to build the pressure up in the reservoir and burst into the external environment, independent of the surrounding conditions.

Figure 3 shows time lapse images illustrative of the electrochemical transport of 15 µl of 0.05 g/l vasopressin for the case of an applied potential of 12 V. In order to clearly illustrate the dispersion pattern, we added 720 nm fluorescent flow tracers to FITC-vasopressin conjugation (see supplemental Movies 1 and 2). On average approximately 23 sec after application of the potential the stored contents begin to be ejected from the reservoir. Figure 3(C) shows when the contents are ejected into air and Fig. 3(D) shows the case for ejection into PBS buffer.

To characterize the ejection volume flow rate as a function applied potential, the dispersion pattern of the fluorescent microspheres was recorded as a function of time. By placing a coverslip at a controlled distance above the ejection point the area of the dispersion could be related to an ejected volume using a simple flat cylinder model. Images were then analyzed and processed using ImageJ (National Institutes of Health, http://rsb.info.nih.gov/ij/) and a self-written MATLAB routine (Mathworks, Natick, MA, USA). The results of these experiments are shown in Fig. 4(A). In all cases the advancing fluid front was traced to a distance of 1 mm, limited by the field of view of the microscope. As can be seen there exists a strong dependence of ejected volume on the applied potential. For the first 25 sec, the maximum (12 V) and minimum (8 V) volumetric rates were 4.19 µl/min and 0.460 µl/min, respectively. As such in addition to reducing the overall ejection time (over passive devices), the electrochemical technique also provides a method for controllably modulating the delivery rate through simple adjustment of the applied potential. By modulating the applied voltage the device could also be adapted to pulsatile delivery (Chung et al. 2008).

3.2 Vasopressin release

Time dependent dose profiles were also characterized using FITC-labeled vasopressin as described above. To perform the experiments a control volume of 15 µl of 100 mM PBS was added on top of the membrane and the vasopressin ejection process was enacted for a prescribed length of time. After terminating the ejection process, 1 µl of sample was extracted from the covering drop (after gentle mixing

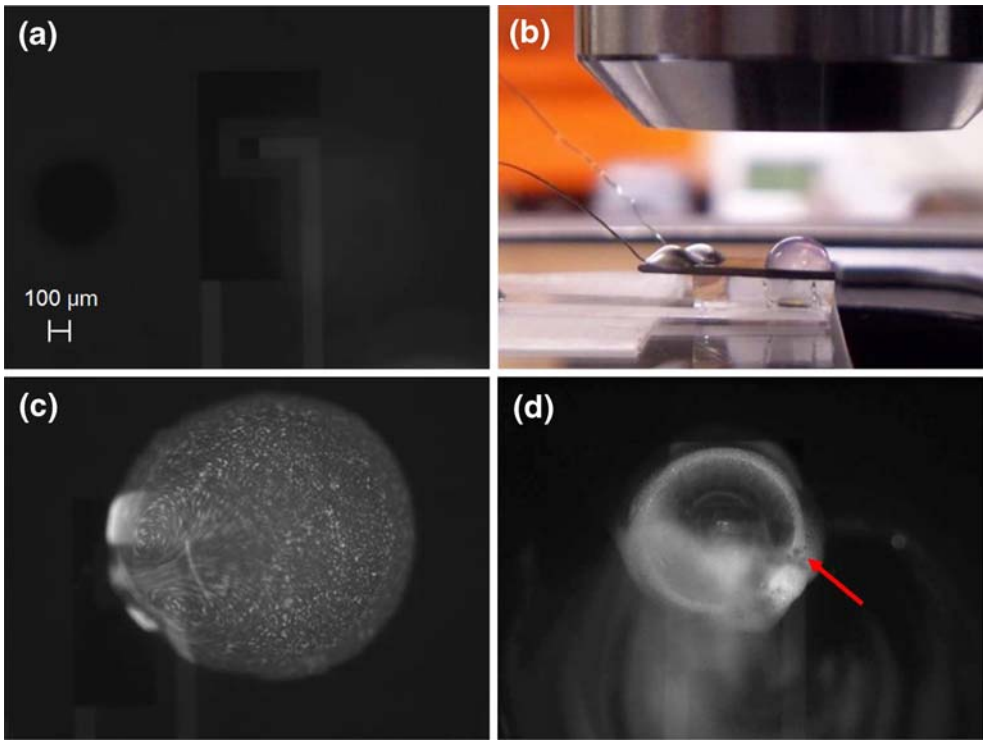

Fig. 3 Illustration showing ejection of vasopressin with 720 nm fluorescent polystyrene microsphere particles from a reservoir. (**a**) Before applying potential. (**b**) Picture of a sample device after ejection into air for five minutes (no initial covering fluid) (**c**) Case 1: Ejection into the air—frame taken one minute after application of 12 V potential (**d**) Case 2: Ejection into PBS buffer—frame taken one minute after application of 12 V potential. The red arrow shows small bubbles release from the well during the ejection process, next to one large bubble in the center region

to ensure homogeneity of the mixture) and dispensed into a 96-well plate for absorbance measurements. The concentration of vasopressin in the drop was determined using the technique described above and the results are plotted in Fig. 4(B). For all experiments, time equals zero was set as the point when the electrochemical reaction was initiated. Analogous to the results presented earlier, Fig. 4(B) also illustrates how increasing the applied potential results in the system reaching the plateau concentration much more rapidly. Note that a relatively low concentration of vasopressin was used in this experiment in order to be compatible with the BCA protein assay. With the current volume of 15 μl, the device is able to deliver maximum of 120 IU (Arg8-vasopressin contains approximately 400 IU/mg (Dawson et al. 1986) and has a solubility of 20 mg/ml). Krismer et al. (2005) reported a set of human cases that where dosages of 100 to 160 IU vasopressin helped to restore spontaneous circulation with sinus rhythm in 2 min. Importantly, the 120 IU limitation of the existing device can be circumvented by parallel integration of devices onto a single chip. This would make it possible to deliver much larger dosages.

Although the focus of this paper is on device design and transport characterization, it is important to briefly discuss the stability of the vasopressin following the electrochemical ejection process. To assess this here we have performed a number of additional mass spectroscopy experiments using MALDI-TOF/TOF (4700 Proteomics Analyzer, Ap-

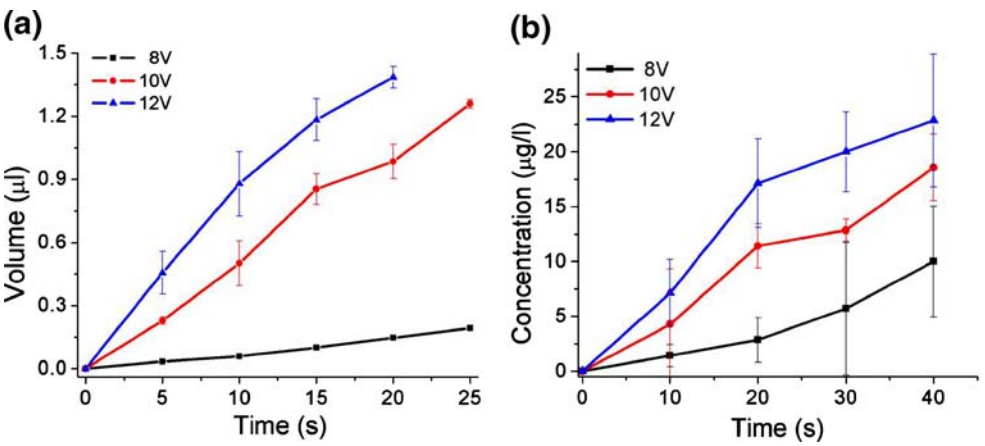

Fig. 4 (**a**) Release rate of vasopressin from sample devices as a function of time for different voltages. (**b**) Concentration profile of vasopressin calculated from BCA protein assay. We set time equals zero as the time when the electrochemical reactions are actuated

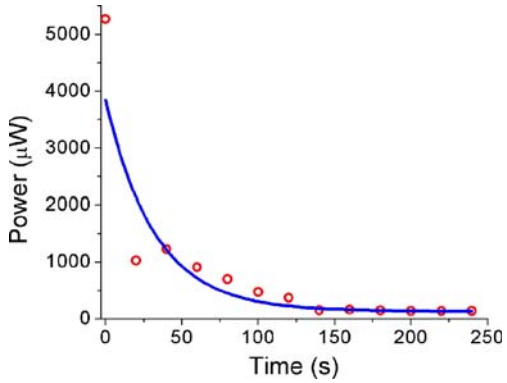

Fig. 5 Representative power load during ejection process for the 12 V case. The line through the data points in this figure represents an exponential best fit. Error bars are not shown since they were smaller than the data marks

plied Biosystems, Foster City, CA, USA). Samples were tested after different electrolytic ejection times using 12 V as the driving voltage, since this represented the harshest conditions we considered in this paper. The details and results of these experiments are presented in the supplemental material (Fig. S1 and associated text) however strong vasopressin peaks (at ~1.085kD) were still observed in the ejected contents after continuous application of the driving potential for 5 min. When compared with the control sample however two additional smaller peaks were also observed at 1.101 kD and 1.117 kD. These two extra peaks are likely oxidation products, suggesting that the electrochemical reaction did cause some degree of degradation to the vasopressin. We are continuing to investigate this observation and hope to better quantify the degradation in the future.

3.3 Power consumption

To determine the power requirements for both the membrane dissolution and electrochemical ejection stages a Keithley 236 Source-Measure Unit was used to monitor the current load. Figure 5 plots a representative case at 12 V where the instantaneous total power consumption was obtained by multiplying the measured current by the applied potential. As can be seen, the power consumption decreases with time, reaching a plateau of around 0.130 mW after 240 sec. For the 12 V case the maximum power load was approximately 5 mW, however this dropped to around 0.9 mW for the 8 V case. This could be further reduced by decreasing the thickness of the PDMS layer, thereby decreasing the distance over which fluid transport must occur and with that the required voltage. Previous studies on similar dose control systems have shown that the electrostatic micropump (Zengerle et al. 1995), thermo-pneumatic (Schomburg et al. 1994), bubble-type planar micropump (Zahn et al. 2004), and ionic conductive polymer film micropump (Guo et al. 1997) techniques require 1 mW with 200 V, 450 mW with 15 V, 18 mW with 10 V, 1000 mW with 40 V and 180 mW with 1.5 V, respectively. In comparison the method represent a good combination of both low voltage requirements and low power consumption.

3.4 Ejection efficiency

The efficiency with which the contents were ejected from the well was quantified by comparing the ratio of the volume loaded into the reservoir with that recovered after the ejection process. In these experiments the recovered volume was calculated in the same manner described in section 3.2. The cumulative amounts of FITC-vasopressin recovered per release for each trial are shown in Fig. 6. The average amount recovered from 10 reservoirs over 5 min when 20 V was applied was 50.3%. The standard deviation among the 10 trials was 6.6%. We expect that this ejection efficiency could be increased by decreasing the thickness of the PDMS layer. This would however result in a lower total dose volume.

4 Conclusion

We have demonstrated here an electrochemically driven, implantable, low power and rate controllable drug delivery device. This approach serves to actively propel the drugs from within a sealed reservoir to the external environment using a combination of electrolytic and gold dissolution reactions induced by the application of a voltage between the top and bottom of the device. The contents dispense rate, concentration profile and power consumption of the device were characterized experimentally. An ejection rate as high as 4.19 μl/min was recorded at a maximum power consumption of roughly 5 mW.

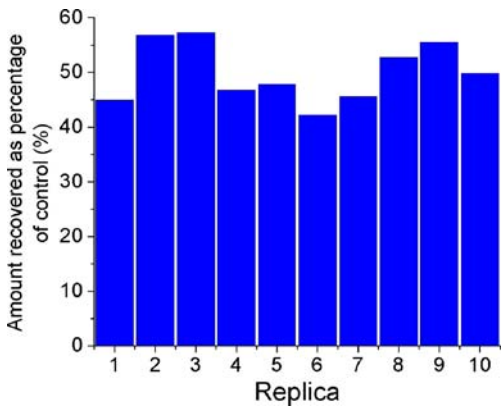

Fig. 6 Release results: total amount of vasopressin recovered over 5 min from each reservoir when 20 V is applied

Acknowledgments This work was supported by the Defense Advanced Research Project Agency, Microsystems Technology Office, Hybrid Insect MEMS (HI-MEMS) program, through the Boyce Thompson Institute for Plant Research. Distribution unlimited. Fundamental research exempt from prepublication controls. The authors would like to thank Donn Kim and Bernardo Cordovez for helpful discussions and technical assistances. The facilities used for this research include Nanoscale Science & Technology Facility (CNF) and Nanobiotechnology Center (NBTC) at Cornell University.

References

A. Ahmed, C. Bonner, T.A. Desai, Biomed. Microdevices. **3**, 89–96 (2001)

A. Ahmed, C. Bonner, T.A. Desai, J. Control, Release **81**, 291–306 (2002)

W.H. Bickell, S.P. Bruttig, G.A. Millnamow, J. Obenar, C.E. Wade, Surgery **110**, 529–536 (1991)

M.C. Belanger, Y. Marois, J. Biomed. Mater. Res. **58**, 467–477 (2001)

A.J. Chung, D. Erickson, Lab chip **9**, 669–676 (2009)

A.J. Chung, D. Kim, D. Erickson, Lab. Chip. **8**, 330–338 (2008)

R.M.C. Dawson, D.C. Elliott, W.H. Elliott, K.M. Jones, *Data for Biochemical Research* (Oxford University Press, Oxford, 1986), p. 31

M.R. Dokmeci, J.A. von Arx, K. Najafi, Proc. Solid-State Sens. Act., Transducers **1**, 283–286 (1997)

E.J. Fitzsimons, J. Sendroy, J. Biol. Chem. **236**, 1595–1601 (1961)

R.P. Frankenthal, D.J. Siconolfi, J. Electrochem. Soc. **129**, 1192–1196 (1982)

A.C.R. Grayson, M.J. Cima, R. Langer, J. Biomed, Mater. Res. A **69A**, 502–512 (2004a)

A.C.R. Grayson, M.J. Cima, R. Langer, Biomaterials **26**, 2137–2145 (2005)

A.C.R. Grayson, R.S. Shawgo, A.M. Johnson, N.T. Flynn, Y.W. Li, M.J. Cima, R. Langer, Proc. IEEE **92**, 6–21 (2004b)

S. Guo, T. Nakamura, T. Fukuda, K. Oguro, Proc. IEEE ICRA, 266-271 (1997)

J.W. Judy, Smart Mat. Struct. **10**, 1115–1134 (2001)

A.C. Krismer, V. Wenzel, W.G. Voelckel, P. Innerhofer, K.H. Stadlbauer, T. Haas, M. Pavlic, H.J. Sparr, K.H. Lindner, A. Koenigsrainer, Anaesthesist **54**, 220–224 (2005)

D.A. LaVan, T. McGuire, R. Langer, Nat. Biotech. **21**, 1184–1191 (2003)

Y.W. Li, H.L.H. Duc, B. Tyler, T. Williams, M. Tupper, R. Langer, H. Brem, M.J. Cima, J. Control, Release **106**, 138–145 (2005)

H.G. Lienhart, K.H. Lindner, V. Wenzel, Curr. Opin. Crit. Care **14**, 247–253 (2008)

K.H. Lindner, A.W. Prengel, E.G. Pfenninger, I.M. Lindner, H.U. Strohmenger, M. Georgieff, K.G. Lurie, Circulation **91**, 215–221 (1995)

M.B. Malay, J.L. Ashton, K. Dahl, S.A. Burchell, R.C. Ashton, R.R. Sciacca, J.A. Oliver, D.W. Landry, Critical Care Medicine **32**, 1327–1331 (2004)

J.M. Maloney, S.A. Uhland, B.F. Polito, N.F. Sheppard, C.M. Pelta, J. T. Santini, J. Control, Release **109**, 244–255 (2005)

G. Milles, C.J. Kouchk, H.G. Zacheis, Surgery **60**, 434–442 (1966)

D. Morales, J. Madigan, S. Cullinane, J. Chen, M. Heath, M. Oz, J.A. Oliver, D.W. Landry, Circulation **100**, 226–229 (1999)

A.B. Peitzman, B.G. Harbrecht, A.O. Udekwu, T.R. Billiar, K. Edward, R.L. Simmons, Curr. Probl. Surg. **32**, 925–1002 (1995)

J.H. Prescott, S. Lipka, S. Baldwin, N.F. Sheppard, J.M. Maloney, J. Coppeta, B. Yomto, M.A. Staples, J.T. Santini, Nat. Biotech. **24**, 437–438 (2006)

B.D. Ratner, A.S. Hoffman, F.J. Schoen, J.E. Lemons, *Biomaterials science: An Introduction to Materials in Medicine* (Academic, San Diego, 2004), pp. 296–304

R.R. Richardson, J.A. Miller, W.M. Reichert, Biomaterials **14**, 627–635 (1993)

I. Roberts, P. Evans, F. Bunn, I. Kwan, E. Crowhurst, Lancet **357**, 385–387 (2001)

J.T. Santini, M.J. Cima, R. Langer, Nature **397**, 335–338 (1999)

W.K. Schomburg, J. Vollmer, B. Bustgens, J. Fahrenberg, H. Hein, W. Menz, J. Micromech, Microeng. **4**, 186–191 (1994)

G.W. Shaftan, C.J. Chiu, C. Dennis, C.S. Grosz, J. Cardiovasc, Surg. **5**, 251–256 (1964)

Y.S. Shin, K. Cho, S.H. Lim, S. Chung, S.J. Park, C. Chung, D.C. Han, J.K. Chang, J. Micromech, Microeng. **13**, 768–774 (2003)

S.A. Stern, S.C. Dronen, P. Birrer, X. Wang, Ann. Emerg. Med. **22**, 155–163 (1993)

W.G. Voelckel, K.G. Lurie, K.H. Lindner, T. Zielinski, S. McKnite, A. C. Krismer, V. Wenzel, Anesth. Analg. **91**, 627–634 (2000)

G. Voskerician, M.S. Shive, R.S. Shawgo, H. von Recum, J.M. Anderson, M.J. Cima, R. Langer, Biomaterials **24**, 1959–1967 (2003)

J.H. Yoo, C. Park, D.H. Hahm, H.J. Lee, H.M. Park, J. Vet, Medical Science **69**, 755–758 (2007)

J.D. Zahn, A. Deshmukh, A.P. Pisano, D. Liepmann, Biomed. Microdevices **6**, 183–190 (2004)

R. Zengerle, J. Ulrich, S. Kluge, M. Richter, A. Richter, Sensor Actuat A-Phys. **50**, 81–86 (1995)